Supplementary Materials for

Discrete Functions of Nuclear Receptor Rev-erbα Couple Metabolism to the Clock

Yuxiang Zhang, Bin Fang, Matthew J. Emmett, Manashree Damle, Zheng Sun, Dan Feng, Sean M. Armour, Jarrett R. Remsberg, Jennifer Jager, Raymond E. Soccio, David J. Steger, and Mitchell A. Lazar1†

†correspondence to: lazar@mail.med.upenn.edu

This PDF file includes:

Materials and Methods

Animal studies

Male wild type inbred C57BL/6 and 129S1/SvlmJ mice were purchased from Jackson Labs. The Rev-erbα knockout mice were obtained from B. Vennström and backcrossed seven or more generations with C57BL/6 mice (*9*). The HDAC3$^{fl/fl}$ mice were described previously (*9*). Mice carrying floxed alleles at Rev-erbα or Rev-erbβ loci were obtained from MCI/ICS (Mouse Clinical Institute—Institut Clinique de la Souris, Illkirch-Graffenstaden; http://www.ics-mci.fr/), as reported previously (*12, 23*). RORα floxed mice were obtained from MCI/ICS, and RORγ floxed mice were obtained from Jackson Laboratory. Mice were housed on a temperature-controlled specific-pathogen free facility with 12:12-hour light–dark cycle (lights on at 07:00, lights off at 19:00). Experiments were carried out on 12–16-week-old male mice. All animal studies were performed with an approved protocol from the University of Pennsylvania Perelman School of Medicine Institutional Animal Care and Use Committee.

ChIP

ChIP experiments were performed as described (*9*) with minor changes. Mouse liver, brain (ventral tegmental area), and epididymal white adipose tissue (eWAT) were harvested, minced and cross-linked in 1% formaldehyde for 20min, followed by quenching with 1/20 volume of 2.5M glycine solution for 5 min, and two washes with 1×PBS. Nuclear extracts were prepared by Dounce homogenization in ChIP buffer (50mM Tris-HCl pH 7.5, 140mM NaCl, 1mM EDTA, 1% Triton X-100, 0.1% NaDOC). Chromatin fragmentation was performed by sonication in lysis buffer (50mM Tris-HCL ph 8.0, 0.1%SDS, 10mM EDTA), using the Bioruptor (Diagenode). Proteins were immune-precipitated in ChIP buffer, and crosslinking was reversed overnight at 65°C in SDS buffer (50mM Tris-HCL, 10mM EDTA, 1% SDS, pH 8), and DNA isolated using phenol/chloroform/isoamyl alcohol. Precipitated DNA was analyzed by quantitative PCR or high-throughput sequencing.

ChIP-Re-ChIP

ChIP-Re-ChIP was performed in essentially the same way as ChIP, except that the first elution was carried out in a reducing elution buffer (1% SDS, 10 mM DTT), shaking at 800 rpm for 15 min at 65°C. The Rev-erbα ChIP eluate was then diluted in ChIP dilution buffer with 5 mg/ml BSA and 2 μg/ml lamda DNA-HindIII digest, divided into two, and subjected to HNF6, Rev-erbα, or IgG ChIP.

Quantitative PCR

Quantitative PCR was performed with Power SYBR Green PCR Mastermix and the PRISM 7500 instrument (Applied Biosystems), and analysis was performed by the standard curve method.

ChIP-seq

ChIP experiments were performed independently on liver samples from individual mice harvested at indicated times. DNA was amplified according to ChIP Sequencing Sample Preparation Guide provided by Illumina, using adaptor oligo and primers from

Illumina, enzymes from New England Biolabs (NEB) and PCR Purification Kit and MinElute Kit from QIAGEN. Deep sequencing was performed by the Functional Genomics Core (J. Schug and K. Kaestner) of the Penn Diabetes Endocrinology Research Center using the Illumina HiSeq2000, and sequences were obtained using the Solexa Analysis Pipeline.

ChIP-seq data processing

Sequencing reads of biological replicates were pooled and aligned to the mm9 genome, followed by peak calling according to previously described (*22*). Genome browser tracks of ChIP-seq data were generated using Homer v4.7 (*30*) and visualized in IGV (*31*). For the comparison of Rev-erbα cistromes in multiple tissues, peaks higher than 1 read per million (rpm) were used, and motifs mining was performed using Homer in 200bp regions surrounding the peak centers. RORα ChIP-seq at ZT22 and liver input were published in earlier studies (*9, 22*). RORα and RORγ liver cistromes were determined by pooling their peaks found at ZT10 and ZT22. To eliminate potential bias from different reading depths, 20 million reads were selected by random sampling from Rev-erbα ChIP-seq data in WT and DBD^m and subjected to downstream analysis. Rev-erbα ChIP-seq in αKO mice (*22*) was also analyzed using the same number of reads to eliminate false positive binding (*6*). Similarly, 10 million randomly sampled reads from HDAC3 ChIP-seq in WT, Rev-erb DBD^m, and Rev-erbαKO/βKD mouse livers were used for the peak height quantification. Among Rev-erbα peaks that are great than 1rpm and at least 3 times stronger than their counterpart in Rev-erbα KO, DBD-dependent Rev-erbα sites were selected using the cutoff: tag count fold change $WT/DBD^m > 3$ or tag count difference $WT\text{-}DBD^m > 3$ rpm; DBD-independent Rev-erbα sites were selected using cutoff: tag count fold change $WT/DBD^m < 1.5$ and $DBD^m/WT < 1.5$. DBD-dependent Rev-erbα sites with reduced HDAC3 binding in DBD^m liver (HDAC3 $WT/DBD^m > 1.5$ and WT>1rpm) were defined as DBD-dependent Rev-erbα/HDAC3 sites. DBD-independent Rev-erbα sites with intact HDAC3 binding in DBD^m liver (HDAC3 $WT/DBD^m < 1.5$ and WT>1rpm) were defined as DBD-independent Rev-erbα/HDAC3 sites. All ChIP-seq peaks were annotated by Homer using the nearest mapping within 50kb of gene TSSs. ChIP-seq data are available in GEO (GSE67973).

SNP mediated strain-specific binding

Rev-erbα ChIP-seq reads from 129 mice were aligned to the mm9 reference genome using GSNAP (*32*), allowing mismatches at ~5.4 million SNPs specific to 129 genome (*33*). To minimize potential bias introduced by different IP efficiency in B6 and 129 mice, Rev-erbα peaks identified in two strains were pooled and their peak heights were quantile normalized prior to the analysis of strain-specific binding. Rev-erbα peaks where Fimo (*34*) predicted HNF6 motif score was altered by the SNP, from one strain to the other, were selected, and the log2 fold change for peak height in two strains was calculated.

ChIP-exo

The ChIP-exo portion of the protocol was performed as described (*20*) with modifications making the assay compatible with the Illumina sequencing platform. Briefly, it was performed in essentially the same way as ChIP-seq, except that after the

end repair, adapter ligation and nick repair, the DNA was digested by the lambda (M0262, NEB) and RecJf exonucleases (M0264, NEB), while it is still on the agarose beads. Then, the DNA samples were eluted from the beads and are analyzed by high-throughput sequencing.

ChIP-exo data processing

Rev-erbα ChIP-exo reads from two biological replicates were pooled and aligned to the mouse genome (mm9) using bowtie (*35*) with parameters '-n 1 and -m 1'. Genome browser track of aligned reads were generated using Homer with the parameter -fragLength 10 and visualized in IGV. ChIP-exo peak call on the forward and reverse strands was performed using MACE-1.0 with default parameter (*21*). The most prevalent ChIP-exo peaks were selected from within published Rev-erbα ChIP-seq peaks (*22*). Two approximate exo-peaks on different DNA strands (a peak pair) with distance from -50bp to +150bp (center of negative strand peak – center of positive strand peak), was found using the windowBed feature of bedtools-2.21 (*36*). Peak pairs with a distance less than +/-2 bp from the most prevalent distance of all peak pairs were selected. Motif search was performed in 30bp regions surrounding the peak pair centers using Homer. HNF6 ChIP-exo (*21*) data were reprocessed using the same protocol. ChIP-exo data are available in GEO (GSE67973).

Analysis of GRO-seq data

Nascent gene and eRNA transcription were determined as previously described (*22*).

Western blot and gene expression analysis

For the western blot of the total lysates, we lysed tissues or cells in radio-immuno-precipitation assay (RIPA) buffer supplemented with phosphatase and protease inhibitors, resolved the samples by Tris-glycine SDS-PAGE, transferred the samples to a nitrocellulose membrane and blotted them with the indicated antibodies. For qRT-PCR, we extracted total RNA using TRIzol (Invitrogen) and a High Pure RNA tissue kit (Roche). We performed qRT-PCR with a High Capacity RT kit, a SYBR Green PCR Master Mix and the PRISM 7500 instrument (ABI) using the absolute quantification method with standard curves. 36B4 (Arbp) was used as housekeeping control.

Microarray Analysis

Liver samples were taken from 12 week old male RORα$^{fl/fl}$γ$^{fl/fl}$ mice 2 week after injection of AAV-Cre or AAV-GFP virus (4 mice per group). Total RNA was extracted from each liver sample using the RNeasy Mini Kit (Qiagen). Each RNA sample was processed with the Ambion WT Expression Kit and the GeneChip WT Terminal Labeling and Controls Kit (Affymetrix), and hybridized to the Mouse Gene 2.0 ST Array (Affymetrix). The array was then read by GCS3000 laser scanner (Affymetrix), and microarray data analysis was carried out using Partek® Genomics Suite software (Copyright, Partek Inc.). Subsequent data analysis was performed using BioConductor. All microarray data were processed using previously described protocol (*22*). ROR target genes were selected using threshold $p<0.01$, expression fold change < -1.3 and compared with Rev-erbα target genes previously identified using equivalent cutoffs (*23*). For comparison between Rev-erbα target genes and DBD^{m} target genes, $p<0.05$ and

expression fold change > 1.3 were used, and only those containing at least one Rev-erbα binding site within 50kb of their TSSs were compared. The procedures were performed by the Penn Molecular Profiling Core. The microarray data for Rev-erbα KO mice and Rev-erbαDBD^{m}/βKO are from previous publications (*9, 12*). Microarray data are available in GEO (GSE67973).

Mass spectrometric identification of Rev-erbα

Rev-erbα antibody (Cell signaling Technology #2124) was covalently linked to AminoLink™ Coupling Resin (Thermo). Tissue was lysed in RIPA with protease inhibitors and sonicated. Cleared lysates were incubated with 100 µl of resin overnight at 4°C, washed in RIPA, eluted in 10% NH_4OH, and dried. Samples were prepared for MS as previously described (*37*). After reduction/alkylation, samples were digested with Lys-C (Wako) followed by trypsin (Promega) at 37°C. Samples were resuspended in 1% acetic acid, and desalted with C_{18} stage tips as previously described (*38*). EASY-nanoLC (Thermo) was configured with a 75 µm ID x 17 cm Reprosil-Pur C18-AQ (3 µm; Dr. Maisch GmbH, Germany) nano-column and coupled with an Orbitrap Fusion mass spectrometer (Thermo). Full scan MS spectrum (m/z 360−1600) was performed in the Orbitrap with a resolution of 120,000 (at 200 m/z). Fragmentation was performed with higher-energy collisional dissociation (HCD) and a maximum injection time of 120 msec. MS/MS data were collected in centroid mode in the ion trap mass analyzer. Peak area was extracted from raw files by using Proteome Discoverer v1.4 and peptides were identified using MASCOT.

Hepatic triglyceride assay

Liver samples were homogenized in the TissueLyser (Qiagen) with steel beads in tissue lysis buffer (140mM NaCl, 50mM Tris and 1% Triton-X, pH8.0). Triglyceride concentration in the lysates was then quantified using LiquiColor Triglyceride Procedure No. 2100 (Stanbio).

Oil Red O staining

5µM frozen sections were prepared from snap-frozen liver tissues. The sections were stained in 0.5% Oil Red O in propylene glycerol overnight for lipid and then in hematoxylin for nucleus for 5 seconds. The procedures were performed by the Penn Digestives Disease Center Morphology Core.

Antibodies

Rev-erbα antibody was purchased from Cell Signaling Technology (#2124). HDAC3 antibodies were purchased from Abcam (ab7030). HNF6 antibody was purchased from Santa Cruz Biotechnology (sc13050). RORα antibody from Santa Cruz Biotechnology (sc6062). RORγ antibody was purchased from Santa Cruz Biotechnology (sc28559).

Constructs and gene transductions

The adeno-associated viruses encoding Cre recombinase (AAV-Cre), GFP (AAV-GFP) and flag-tagged Rev-erbα were obtained from the Vector Core of the Penn Diabetes Research Center. The *Cre*, *GFP* or flag-taggered *Rev-erbα* gene was inserted

into the AAV2/8 vector containing the liver specific Tbg promoter. Each 12 week old male floxed mouse received 1.5 $\times 10^{11}$ particles of virus through tail-vein injection. The adenoviruses encoding shRNA targeting the β-galactosidase (TGCACCTGGTAAATCTTAT) or the Rev-erbβ gene (GCACTAAGGACCTTA ATAATG) were constructed using the BLOCK-iTadenoviral RNAi expression system from Invitrogen (#K4941-00) and subsequently amplified and purified by the Vector Core, as described previously (*6*). Each mouse received 5.7×10^{11} particles of virus through tail vein injection.

Biological processes	P value
Genes bound by common sites	
rhythmic process	3.14E-04
circadian rhythm	1.43E-03
regulation of biosynthetic process	5.13E-03
regulation of macromolecule biosynthetic process	6.37E-03
regulation of metabolic process	6.63E-03
Genes bound by liver specific sites	
oxoacid metabolic process	3.59E-11
carboxylic acid metabolic process	3.59E-11
organic acid metabolic process	3.78E-11
cellular ketone metabolic process	6.62E-11
steroid metabolic process	3.38E-10
Genes bound by brain specific sites	
regulation of cell communication	5.43E-13
regulation of signal transduction	1.09E-11
regulation of small GTPase mediated signal transduction	2.48E-08
anatomical structure development	2.44E-07
regulation of Ras protein signal transduction	2.83E-07
Genes bound by eWAT specific sites	
positive regulation of cellular process	3.04E-04
brown fat cell differentiation	4.80E-04
positive regulation of biological process	6.06E-04
regulation of foam cell differentiation	9.61E-04
regulation of cell adhesion	0.001299

Fig. S1.

Rev-erbα cistrome in different tissues. Gene ontology analysis for genes bound by shared Rev-erbα binding sites among tissues and those bound by tissue specific Rev-erbα sites (1000 genes with most tissue-specific binding sites were used).

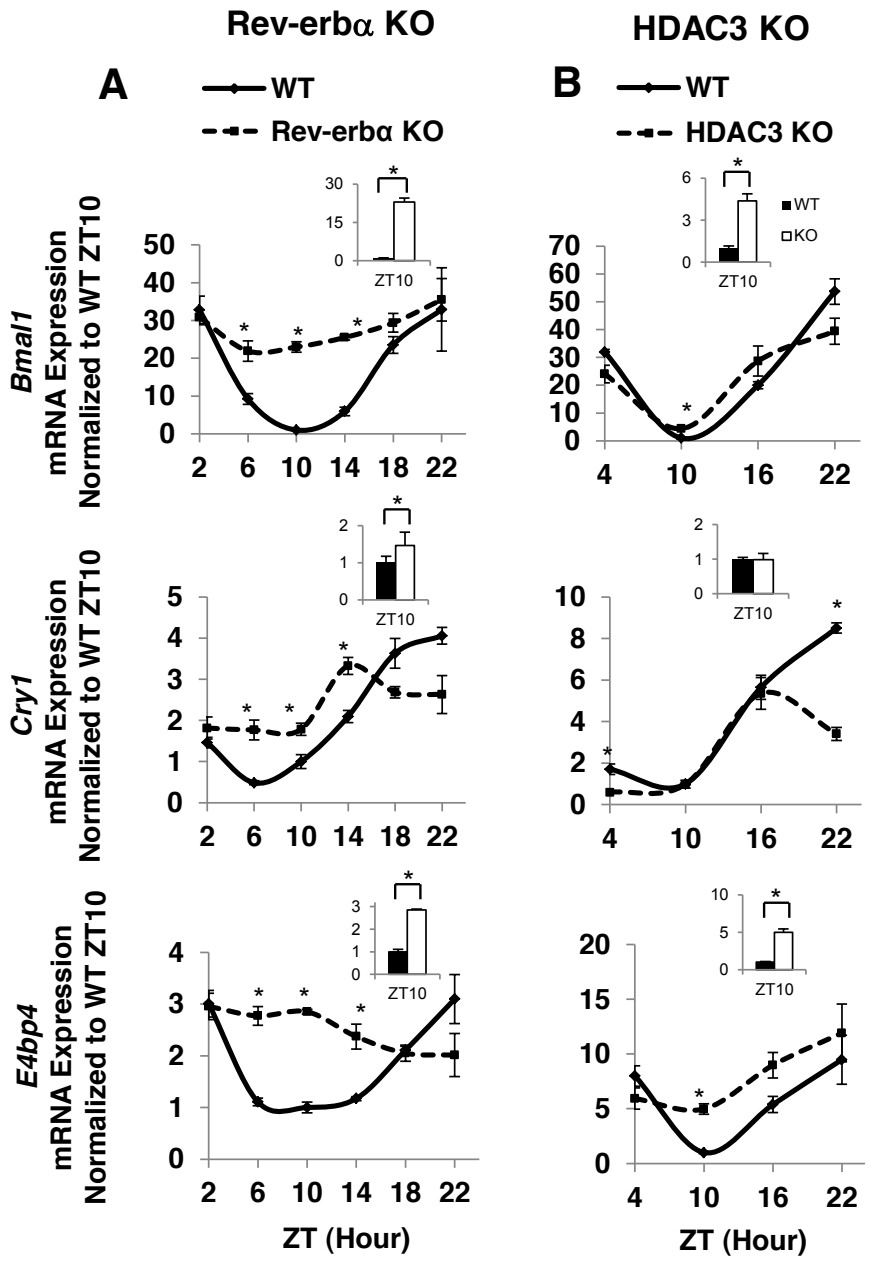

Fig. S2

HDAC3 does not dampen circadian rhythmicity of clock genes. mRNA expression of *Bmal1*, *Cry1,* and *E4bp4* over a 24-hour period in wild type, Rev-erbα knockout and HDAC3 KO mouse liver. The expression at ZT10 is highlighted in the upper right corner of the plot. Data are expressed as mean± SEM (* Student's t-test, $p < 0.05$, n= 4 or 5 per group).

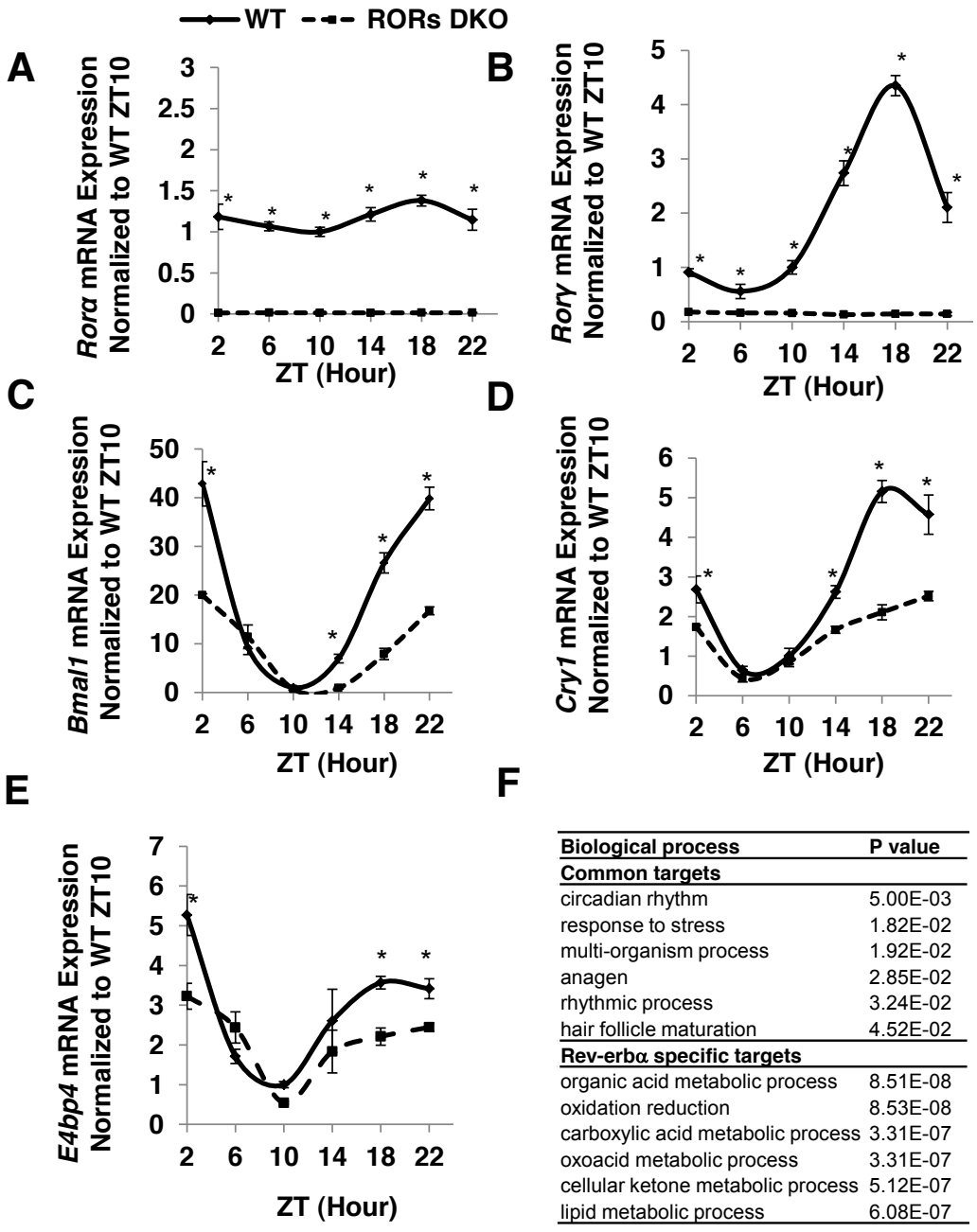

Biological process	P value
Common targets	
circadian rhythm	5.00E-03
response to stress	1.82E-02
multi-organism process	1.92E-02
anagen	2.85E-02
rhythmic process	3.24E-02
hair follicle maturation	4.52E-02
Rev-erbα specific targets	
organic acid metabolic process	8.51E-08
oxidation reduction	8.53E-08
carboxylic acid metabolic process	3.31E-07
oxoacid metabolic process	3.31E-07
cellular ketone metabolic process	5.12E-07
lipid metabolic process	6.08E-07

Fig. S3

RORs are necessary for robust circadian rhythm of clock gene expression. (A to E) mRNA expression of *Rorα, Rorγ, Bmal1, Cry1,* and *E4bp4* over a 24-hour period in wild type and RORs double knockout mice. Data are expressed as mean ± SEM (* Student's t-test, $p < 0.05$, n= 4 or 5 per group). (F) Gene ontology analysis using RORs/Rev-erbα common target genes or Rev-erbα specific targets.

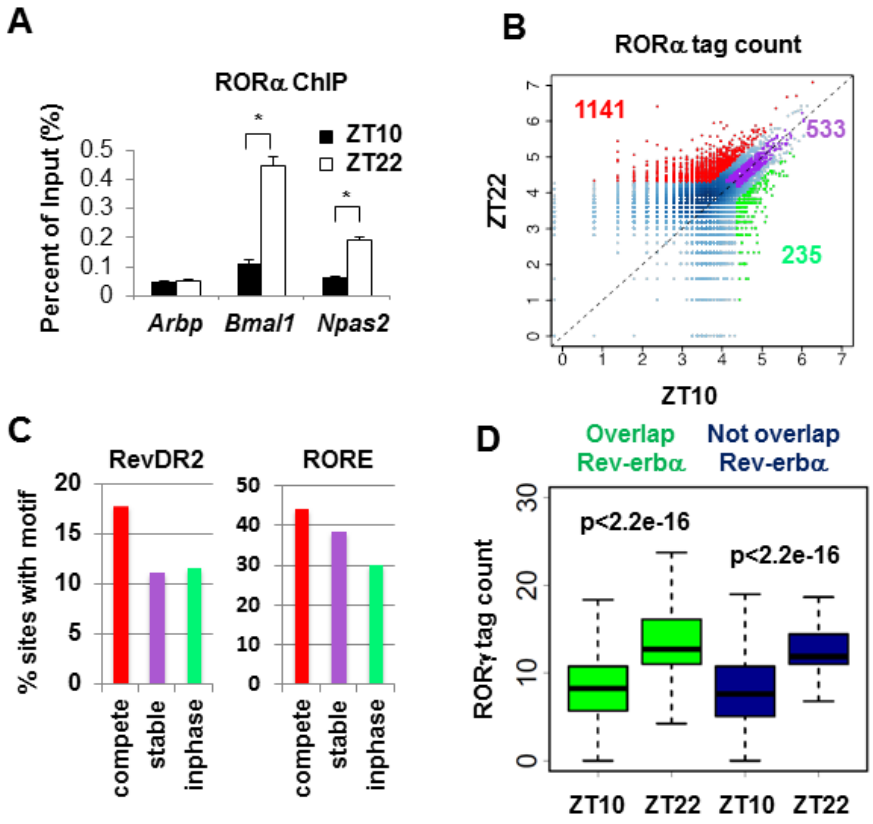

Fig. S4

RORs control clock gene expression through oscillating binding. (A) ChIP-PCR validation of cyclic RORα binding at clock genes promoters at ZT10 or ZT22 in wild type mice liver, in comparison with an unbound control at *Arbp*. Data are expressed as mean ± SEM (Student's t-test, *p<0.05, n=4). (B) Binding strength of RORα at overlapped site with Rev-erbα. High-confidence RORα sites (>2rpm) oscillating in opposite phase to the binding of Rev-erbα (compete sites, red, tag count ZT22/ZT10>1.5) are compared with stable sites (purple, tag count fold change<1.2) and sites oscillating in the same phase as Rev-erbα (inphase sites, green, tag count ZT10/ZT22>1.5). (C) Enrichment of RevDR2 and RORE motifs in three groups of RORα sites from B. (D) Oscillating binding strength of RORγ at sites overlap, or not overlap with Rev-erbα cistromes (P values are from Student's t-test).

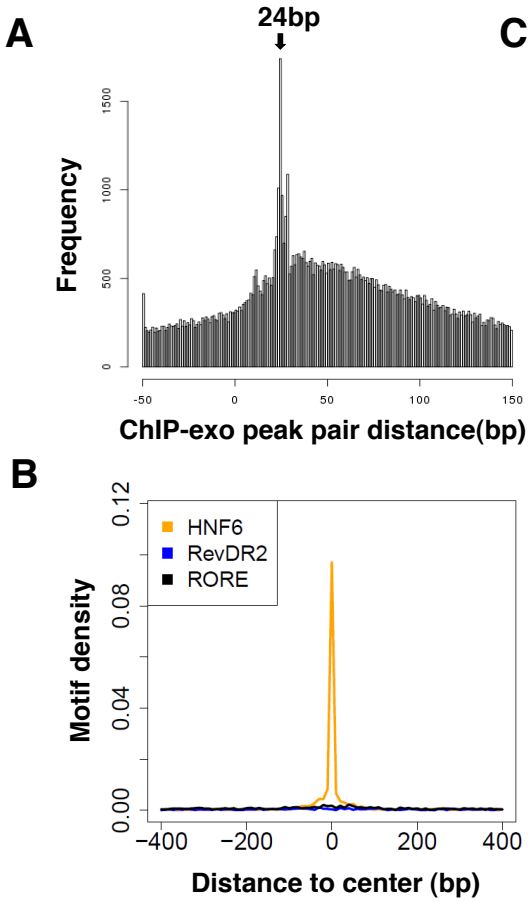

C

Gene ontology of the genes near Rev-erbα/HNF6-exo sites

Biological Process	P value
Lipid metabolic process	8.64E-5
Steroid metabolic process	9.57E-4
Cellular lipid metabolic process	1.85E-3
Regulation of biological quality	2.81E-3
Homeostatic process	4.80E-3

Fig. S5

Rev-erbα ChIP-exo sites are enriched for HNF6 motif. (A) Distance distribution for Rev-erbα ChIP-exo peak pairs, identified by MACE (*22*). The most frequently observed distance is 24bp. (B) Density of selected motifs centered at Rev-erbα ChIP-exo sites with peak pair distance of 24bp. (C) Gene ontology for genes closest to Rev-erbα/HNF6-exo sites.

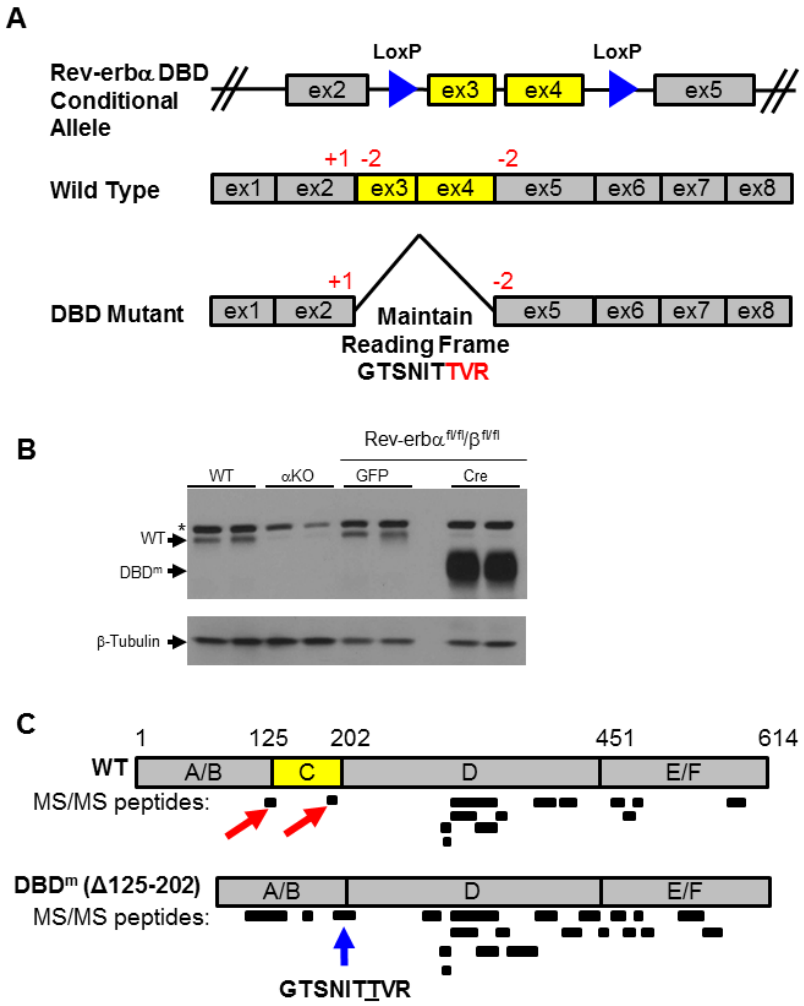

Fig. S6

Conditional Rev-erbα allele deletion results in an in-frame DNA binding domain mutant (DBD^m). (A) Illustration depicting floxed exons 3 and 4 encoding the DNA binding domain of the Rev-erbα locus. Numbers highlighted in red represent the nucleotide codon phases at exon-exon junctions. Deletion of exons 3 and 4 maintains the open reading frame through splicing of exon 2 to exon 5. The peptide sequence highlighted (from S6C) is unique to the conditional Rev-erbα DBD^m, with amino acids encoded in exons 2 and 5 colored black and red respectively. (B) Western blot of Rev-erbα in the livers of wild type mice, Rev-erbα KO mice, wild type control mice (floxed mice injected with AAV-GFP), and DBD^m mice (floxed mice injected with AAV-Cre), "*" denotes non-specific band. (C) Rev-erbα peptides detected by mass spectrometry in wild type control and the DBD^m livers. Red arrows indicate peptides discovered in wild type control liver mapping to the DNA binding domain of Rev-erbα, which are absent in the DBD^m. The blue arrow indicates a unique peptide found only in the DBD^m livers as a result of the new open reading frame joining exons 2 and 5. Note the third threonine (amino acid 203) of the highlighted DBD^m peptide is a 1 amino acid substitution from alanine resulting from the new exon splice junction between exons 2 and 5.

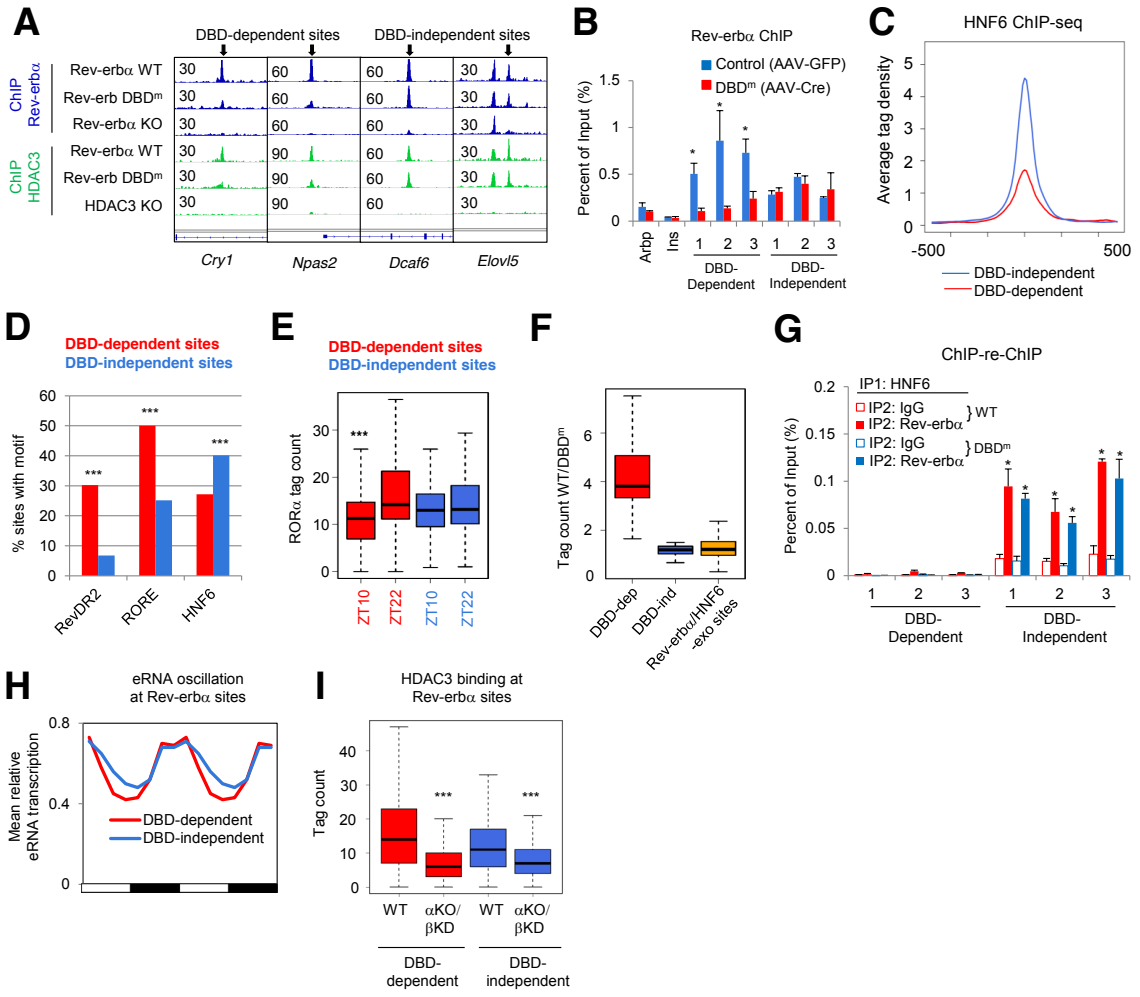

Fig. S7

Rev-erbα DBD-independent sites are enriched for HNF6 binding. (A) Genome browser view of Rev-erbα and HDAC3 binding in wild type, Rev-erbα DBD^{m}, and KO mice. (B) Binding strength of Rev-erbα at selected DBD-dependent and DBD-independent sites at ZT10 as determined by ChIP-PCR. Data are expressed as mean±SEM (* Student's t-test, $p < 0.05$, n=4 per group). (C) HNF6 tag density at Rev-erbα DBD-dependent and -independent sites. (D) The percent of sites containing RevDR2, RORE, or HNF6 motif in DBD-dependent sites and DBD-independent sites (*** hypergeometric test p<1e-3). (E) Circadian binding of RORα at Rev-erbα DBD-dependent sites but not DBD-independent sites (*** Student's t-test p<1e-3). (F) Difference in Rev-erbα binding strengths between WT and DBD^{m} mice at three groups of binding sites. (G) Sequential ChIP of HNF6 followed by either Rev-erbα or IgG ChIP in wild type and DBD^{m} mouse liver at ZT10. Data are expressed as mean±SEM (* Student's t-test, p<0.05, n=3 or 4 per group). (H) eRNA oscillation at DBD-dependent sites and DBD-independent sites throughout 24-hour light dark cycle. Time points were duplicated for better visualization. (I) Comparison of HDAC3 binding in WT and Rev-erb αKO/βKD mice (*6*) at DBD-dependent and DBD-independent Rev-erbα sites.

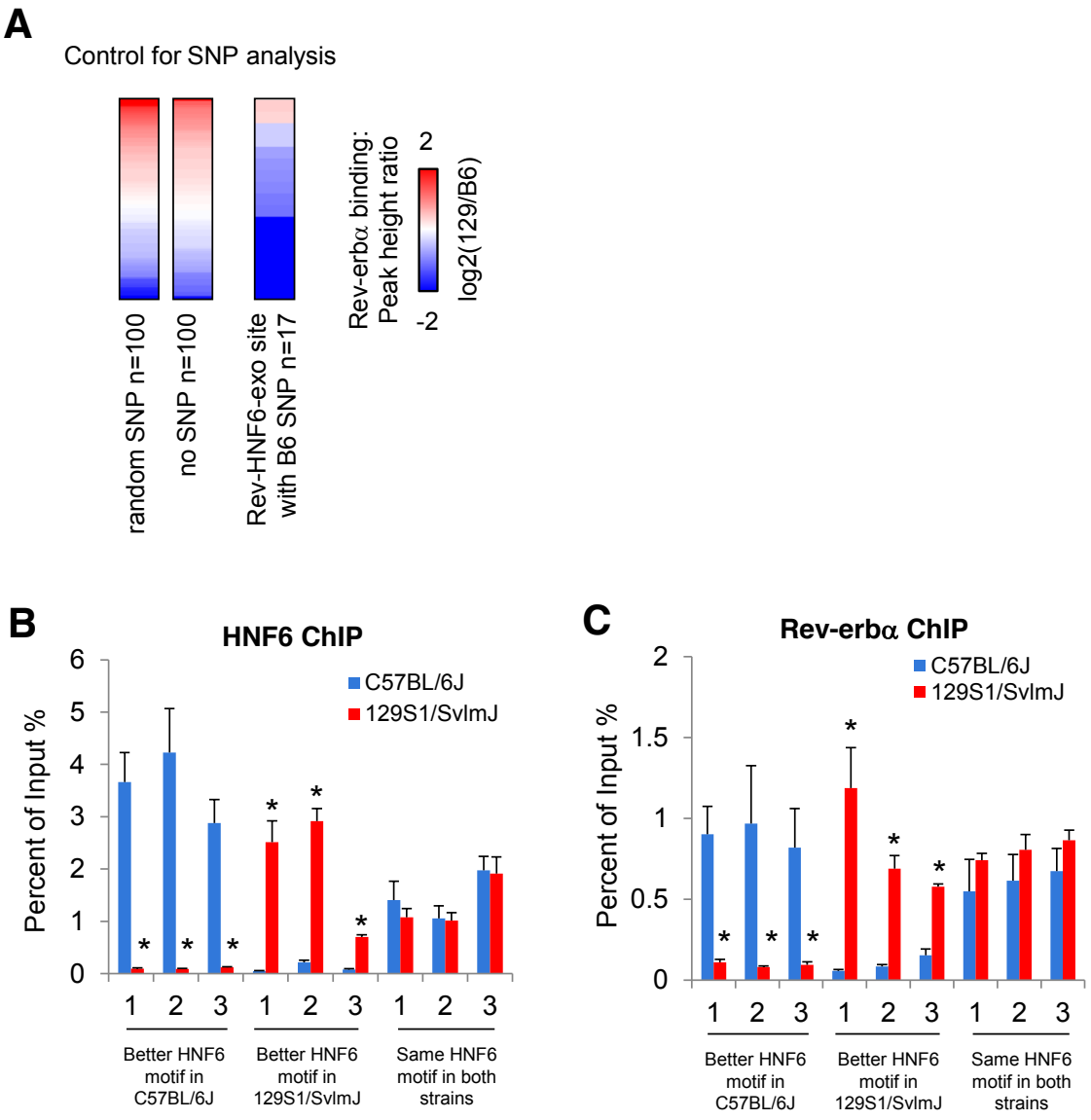

Fig. S8

Binding strength of Rev-erbα in C57BL/6J and 129S1/SvlmJ. (A) Difference in binding strength of Rev-erbα in 129 and B6 mice, at 100 Rev-erbα binding sites containing random SNPs (left column), without SNP (middle column), or at 17 Rev-erbα/HNF6-exo sites with B6 HNF6 motifs being disrupted in 129 mice due to the SNPs (right column). (B-C) Binding strengths of HNF6 (B) and Rev-erbα (C) are correlated with HNF6 motif at selected Rev-erbα sites at ZT10, as determined by ChIP-PCR. Data are expressed as mean± SEM (* Student's t-test, $p < 0.05$, n=4 per group).

A

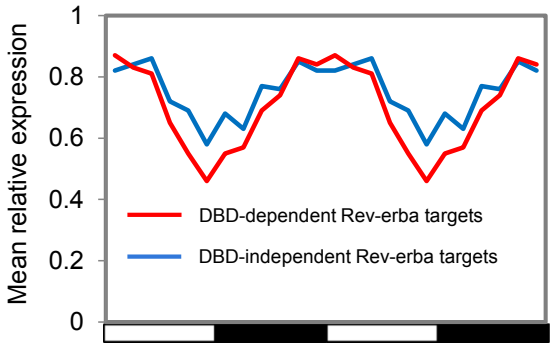

B

Top Gene Ontology Term	
DBD-independent Rev-erbα targets	**DBD-dependent Rev-erbα targets**
Oxoacid Metabolic Process	Steroid Biosynthetic Process
Carboxylic Acid Metabolic Process	Negative Regulation of Apoptosis
Organic Acid Metabolic Process	Negative Regulation of Programmed Cell Death
Cellular Ketone Metabolic Process	Negative Regulation of Cell Death
Monocarboxylic Acid Metabolic Process	Response to Toxin
Cellular Lipid Metabolic Process	Lipid Biosynthetic Process
Fatty Acid Metabolic Process	Rhythmic Process
Lipid Metabolic Process	Circadian Rhythm

C

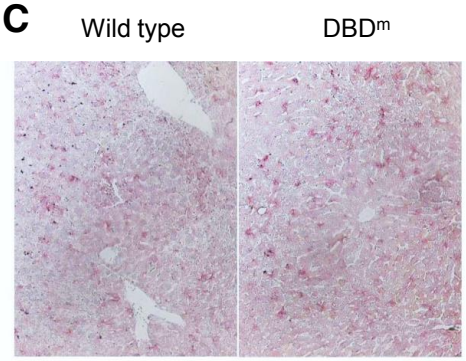

Fig. S9

Genes regulated exclusively in Rev-erbα KO are enriched for metabolic process. (A) Circadian average mRNA expression of Rev-erbα DBD-dependent and -independent target genes in Fig. 4A. mRNA levels throughout 24-hour cycle were normalized to the peak expression of the day. Time course microarray data from (*39*) were duplicated for better visualization. (B) Gene ontology analyses for Rev-erbα DBD-dependent and -independent target genes. (C) Oil Red O staining of livers from wild type control mice (Rev-erbα/β floxed mice injected with AAV-GFP), and DBD^{m} mice (Rev-erbα/β floxed mice injected with AAV-Cre).

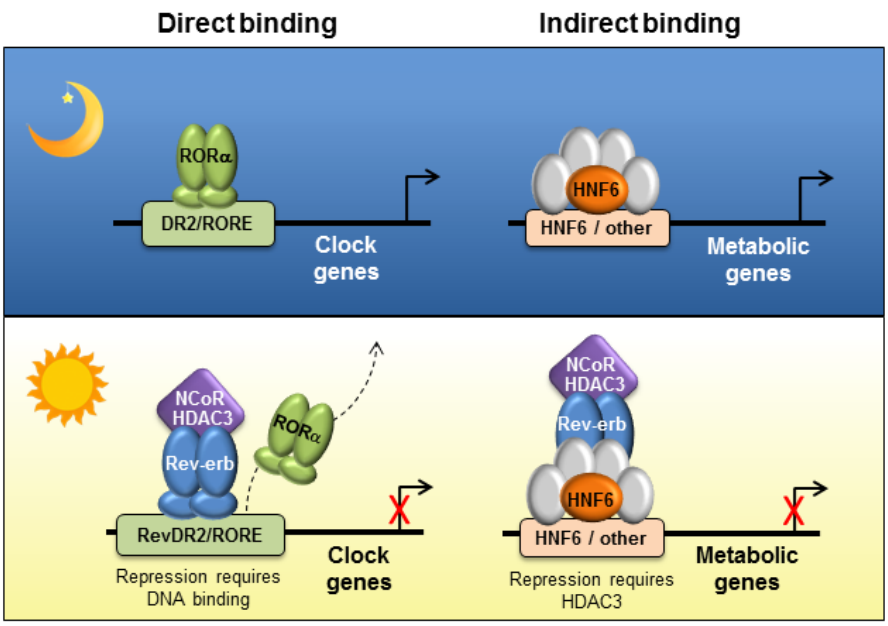

Fig. S10

Model depicting distinct mechanisms of Rev-erbα regulating clock and metabolic genes in liver. Grey refers to other potential TFs that may be involved in the tethering of Rev-erbα.

Table S1.

Primers used for ChIP-qPCR and RT-qPCR.

ChIP-qPCR Primers		
Site Name	**Forward Primer**	**Reverse Primer**
Arbp	GAGGTGGCTTTGAACCAGAG	TCTTTGTCTCTGTCTCGGAAAA
Insulin	GGACCCACAAGTGGAACAAC	GTGCAGCACTGATCCACAAT
Bmal1	AGCGGATTGGTCGGAAAGT	ACCTCCGTCCCTGACCTACT
Npas2	CTGTCTTGGCTAGGGGTTTG	GAGACAGGCGAGAATCCAAG
DBD dependent site 1	GAGATTGGGTCACCACAGGT	GTGACCCAGCCACCTATGAC
DBD dependent site 2	ATTCCCTACTGCCCCAATTC	TTGTCCCACTCAAACAGCAG
DBD dependent site 3	TGTCTCCTCCCACAGGAAAA	CACTGCCCTCTCTCCTTTTG
DBD independent site 1	TAGGGCTCTGCAGATTAGCC	GCCCATGTGAAAATGGATGT
DBD independent site 2	CCCTGGAAGTATAAGCGAGACA	GGGTTCAGGGTTCCATTCTT
DBD independent site 3	CATGCAATCGCTGACAGAAT	AAGGGGTATGGAGTCGGAGT
Better HNF6 motif in C57BL/6J site 1	TCCCAGTGTGAAGGTTTTGTT	GCTTGATGATGTGGCTGAGA
Better HNF6 motif in C57BL/6J site 2	TTTCCGTGTTGTGTGTTTTCA	AAGCGCTAATTGAGCAAATCA
Better HNF6 motif in C57BL/6J site 3	GACGATTTGCCATGTTTCCT	CATGTTCTCTCTGCCGAGGT
Better HNF6 motif in 129S1/SvlmJ site 1	TGATAAATCCCTGGCCTTTG	GCAGAGCTGCTTGGAAAGTC
Better HNF6 motif in 129S1/SvlmJ site 2	TTCCGGGAGAAACTGTAAGC	GGGTATCGATTTGACCCGTA
Better HNF6 motif in 129S1/SvlmJ site 3	GGATGCAGAAGCAGCAATAA	CTGCTGACACTGAACCAGGA
Same HNF6 motif in both strains site 1	TGAGACCAAGGCTCAAAAGAA	ACAAAGTGCACAGCTTGGAA
Same HNF6 motif in both strains site 2	CAGTGGCAATGCTTCTGTGT	TTGCAGCTGGACTCTGAGC
Same HNF6 motif in both strains site 3	TGAACCCTGTAAAGCAGACCA	CCCGTACCGTTCCTGTAGTC
RT-qPCR Primers		
Site Name	**Forward Primer**	**Reverse Primer**
Arbp	TCCAGGCTTTGGGCATCA	CTTTATCAGCTGCACATCACTCAGA
Bmal1	TAGGATGTGACCGAGGGAAG	TCAAACAAGCTCTGGCCAAT
Cry1	AGCGCAGGTGTCGGTTATGAGC	ATAGACGCAGCGGATGGTGTCG
E4bp4	GCTCTTTTGTGGACGAGCAT	ACCGAGGACACCTCTGACAC
RORα	TGTTTGATTGATCGGACCAG	CTTGGACATCCCGACCAAACT
RORγ	ACTACGGGGTTATCACCTGTGAG	GTGCAGGAGTAGGCCACATTAC
Cd36	CCACAGTTGGTGTGTTTTATCC	TCAATTATGGCAACTTTGCTT
Plin2	AAGAGGCCAAACAA-AAGAGCCAGGAGACCA	ACCCTGAATTTTCTG-GTTGGCACTGTGCAT
Elovl5	GAACATTTCGATGCGTCACT	GGATGTAATTGTCCAGGAGGA
Acss3	AATGTCGCAAAGTAACAGGCG	GTGGGTCTTGTACTCACCACC

References and Notes

1. D. Feng, M. A. Lazar, Clocks, metabolism, and the epigenome. *Mol. Cell* **47**, 158-167 (2012)
2. G. Asher, P. Sassone-Corsi, Time for food: The intimate interplay between nutrition, metabolism, and the circadian clock. *Cell* **161**, 84-92 (2015)
3. J. S. Takahashi, H. K. Hong, C. H. Ko, E. L. McDearmon, The genetics of mammalian circadian order and disorder: Implications for physiology and disease. *Nat. Rev. Genet.* **9**, 764-775 (2008)
4. J. Bass, J. S. Takahashi, Circadian integration of metabolism and energetics. *Science* **330**, 1349-1354 (2010)
5. P. E. Hardin, S. Panda, Circadian timekeeping and output mechanisms in animals. *Curr. Opin. Neurobiol.* **23**, 724-731 (2013)
6. A. Bugge *et al.*, Rev-erbα and Rev-erbβ coordinately protect the circadian clock and normal metabolic function. *Genes Dev.* **26**, 657-667 (2012)
7. N. Preitner *et al.*, The orphan nuclear receptor Rev-erbα controls circadian transcription within the positive limb of the mammalian circadian oscillator. *Cell* **110**, 251-260 (2002)
8. L. J. Everett, M. A. Lazar, Nuclear receptor Rev-erbα: Up, down, and all around. *Trends Endocrinol. Metab.* **25**, 586-592 (2014)
9. D. Feng *et al.*, A circadian rhythm orchestrated by histone deacetylase 3 controls hepatic lipid metabolism. *Science* **331**, 1315-1319 (2011)
10. Z. Gerhart-Hines *et al.*, The nuclear receptor Rev-erbα controls circadian thermogenic plasticity. *Nature* **503**, 410-413 (2013)
11. E. Woldt *et al.*, Rev-erb-α modulates skeletal muscle oxidative capacity by regulating mitochondrial biogenesis and autophagy. *Nat. Med.* **19**, 1039-1046 (2013)
12. H. Cho *et al.*, Regulation of circadian behaviour and metabolism by Rev-erb-α and Rev-erb-β. *Nature* **485**, 123-127 (2012)
13. L. Yin, M. A. Lazar, The orphan nuclear receptor Rev-erbα recruits the N-CoR/histone deacetylase 3 corepressor to regulate the circadian Bmal1 gene. *Mol. Endocrinol.* **19**, 1452-1459 (2005)
14. V. Giguere *et al.*, Isoform-specific amino-terminal domains dictate DNA-binding properties of ROR alpha, a novel family of orphan hormone nuclear receptors. *Genes Dev.* **8**, 538-553 (1994)
15. B. M. Forman *et al.*, Cross-talk among ROR alpha 1 and the Rev-erb family of orphan nuclear receptors. *Mol. Endocrinol.* **8**, 1253-1261 (1994)
16. H. P. Harding, M. A. Lazar, The monomer-binding orphan receptor Rev-erb represses transcription as a dimer on a novel direct repeat. *Mol. Cell. Biol.* **15**, 4791-4802 (1995)
17. E. Stashi *et al.*, SRC-2 is an essential coactivator for orchestrating metabolism and circadian rhythm. *Cell Rep.* **6**, 633-645 (2014)
18. L. A. Solt, T. P. Burris, Action of RORs and their ligands in (patho)physiology. *Trends Endocrinol. Metab.* **23**, 619-627 (2012)
19. Y. Takeda, R. Jothi, V. Birault, A. M. Jetten, RORgamma directly regulates the circadian expression of clock genes and downstream targets in vivo. *Nucleic Acids Res.* **40**, 8519-8535 (2012)

20. H. S. Rhee, B. F. Pugh, Comprehensive genome-wide protein-DNA interactions detected at single-nucleotide resolution. *Cell* **147**, 1408-1419 (2011)
21. L. Wang *et al.*, Mace: Model based analysis of ChIP-exo. *Nucleic Acids Res.* **42**, e156 (2014)
22. B. Fang *et al.*, Circadian enhancers coordinate multiple phases of rhythmic gene transcription in vivo. *Cell* **159**, 1140-1152 (2014)
23. M. T. Lam *et al.*, Rev-erbs repress macrophage gene expression by inhibiting enhancer-directed transcription. *Nature* **498**, 511-515 (2013)
24. A. J. Faure *et al.*, Cohesin regulates tissue-specific expression by stabilizing highly occupied cis-regulatory modules. *Genome Res.* **22**, 2163-2175 (2012)
25. N. Heldring *et al.*, Multiple sequence-specific DNA-binding proteins mediate estrogen receptor signaling through a tethering pathway. *Mol. Endocrinol.* **25**, 564-574 (2011).
26. C. K. Glass, K. Saijo, Nuclear receptor transrepression pathways that regulate inflammation in macrophages and T cells. *Nat. Rev. Immunol.* **10**, 365-376 (2010).
27. L. Yin *et al.*, Rev-erbα, a heme sensor that coordinates metabolic and circadian pathways. *Science* **318**, 1786-1789 (2007)
28. S. Raghuram *et al.*, Identification of heme as the ligand for the orphan nuclear receptors Rev-erbα and Rev-erbβ. *Nat. Struct. Mol. Biol.* **14**, 1207-1213 (2007)
29. Materials and methods are available as supplementary materials on science online.
30. S. Heinz *et al.*, Simple combinations of lineage-determining transcription factors prime cis-regulatory elements required for macrophage and b cell identities. *Mol. Cell* **38**, 576-589 (2010)
31. J. T. Robinson *et al.*, Integrative genomics viewer. *Nat. Biotechnol.* **29**, 24-26 (2011)
32. T. D. Wu, S. Nacu, Fast and SNP-tolerant detection of complex variants and splicing in short reads. *Bioinformatics* **26**, 873-881 (2010)
33. T. M. Keane *et al.*, Mouse genomic variation and its effect on phenotypes and gene regulation. *Nature* **477**, 289-294 (2011)
34. C. E. Grant, T. L. Bailey, W. S. Noble, Fimo: Scanning for occurrences of a given motif. *Bioinformatics* **27**, 1017-1018 (2011)
35. B. Langmead, C. Trapnell, M. Pop, S. L. Salzberg, Ultrafast and memory-efficient alignment of short DNA sequences to the human genome. *Genome Biol.* **10**, R25 (2009)
36. A. R. Quinlan, I. M. Hall, Bedtools: A flexible suite of utilities for comparing genomic features. *Bioinformatics* **26**, 841-842 (2010)
37. S. M. Armour *et al.*, A high-confidence interaction map identifies SIRT1 as a mediator of acetylation of USP22 and the SAGA coactivator complex. *Mol. Cell. Biol.* **33**, 1487-1502 (2013)
38. J. Rappsilber, Y. Ishihama, M. Mann, Stop and go extraction tips for matrix-assisted laser desorption/ionization, nanoelectrospray, and LC/MS sample pretreatment in proteomics. *Anal. Chem.* **75**, 663-670 (2003)
39. R. Zhang *et al.*, A circadian gene expression atlas in mammals: Implications for biology and medicine. *Proc. Natl. Acad. Sci. U. S. A.* **111**, 16219-16224 (2014)